Gravity-wave forcing in the stratosphere: Observational constraints from the Upper Atmosphere Research Satellite and implications for parameterization in global models

M. Joan Alexander
Colorado Research Associates, Division of Northwest Research Associates, Boulder, Colorado, USA

Karen H. Rosenlof
NOAA Aeronomy Laboratory, Boulder, Colorado, USA

Received 2 January 2003; revised 23 May 2003; accepted 6 June 2003; published 2 October 2003.

[1] Global models that include parameterized gravity-wave effects have an excessively broad range of tuning parameters to choose from that allow a very broad range of gravity-wave momentum forcing distributions. We derive a set of constraints on gravity-wave characteristics near the tropopause from databased estimates of gravity-wave effects in the stratosphere. We use 5.6 years of Upper Atmosphere Research Satellite data and UK Met Office-analyzed wind and temperature fields to first derive estimates of the gravity-wave mean flow forcing in the stratosphere. We then compare these estimates to a suite of gravity-wave model calculations to infer the constraints on the gravity-wave characteristics near the tropopause. These constraints apply to the portion of the gravity-wave spectrum that dissipates in the stratosphere and does not include those that dissipate and drive the mesosphere. We focus on equatorial and extratropical regions separately and find substantially different wave characteristics between the two. We also find a seasonal variation in gravity-wave characteristics in the extratropics. Near the equator, gravity waves assist in driving the quasibiennial and semiannual oscillations, and our constraints on "gravity waves" likely include a blend of characteristics of both ordinary gravity waves and some Kelvin-wave modes. In the extratropics, gravity-wave forcing primarily assists in the annual winter-to-summer transition from westward-to-eastward winds. *INDEX TERMS:* 0341 Atmospheric Composition and Structure: Middle atmosphere—constituent transport and chemistry (3334); 3319 Meteorology and Atmospheric Dynamics: General circulation; 3334 Meteorology and Atmospheric Dynamics: Middle atmosphere dynamics (0341, 0342); 3362 Meteorology and Atmospheric Dynamics: Stratosphere/troposphere interactions; 3384 Meteorology and Atmospheric Dynamics: Waves and tides; *KEYWORDS:* stratosphere, gravity wave, global circulation

Citation: Alexander, M. J., and K. H. Rosenlof, Gravity-wave forcing in the stratosphere: Observational constraints from the Upper Atmosphere Research Satellite and implications for parameterization in global models, *J. Geophys. Res.*, *108*(D19), 4597, doi:10.1029/2003JD003373, 2003.

1. Introduction

[2] Gravity waves are an important mechanism for vertical momentum transport in global circulation models (GCMs), and they can have substantial effects on the circulation and thermal structure of the atmosphere [*Lindzen*, 1973; *Garcia and Boville*, 1994; *Pawson*, 2000]. In the upper troposphere and lower stratosphere, gravity-wave drag on jet stream winds is believed to be an important forcing term in the horizontal momentum equations [*Palmer et al.*, 1986; *McFarlane*, 1987; *Bacmeister*, 1993; *Butchart and Austin*, 1998]. Gravity-wave forcing throughout the stratosphere is also likely to contribute to the strength and seasonal variation in the zonal mean meridional transport circulation [*Alexander and Rosenlof*, 1996]. GCMs tend to have particular trouble in describing the spring-to-summer transition of extratropical winds and temperatures in the stratosphere [*Hamilton et al.*, 1999] and the associated strength of the transport circulation. Gravity-wave forcing is also believed to be important in driving the equatorial quasibiennial and semiannual oscillations (QBO and SAO, respectively) in the stratosphere [*Dunkerton*, 1982; *Jackson and Gray*, 1994; *Dunkerton*, 1997; *Scaife et al.*, 2000].

[3] Atmospheric gravity waves can have horizontal wavelengths ranging from tens to thousands of km and vertical wavelengths ranging from less than 1 km to many tens of km. Their allowed intrinsic frequencies range from the inertial frequency to the buoyancy frequency, and ground based periods can have an even larger range of values. (The intrinsic frequency is that which would be measured by an observer moving with the background

0148-0227/03/2003JD003373$09.00

wind. See (12).) Gravity-wave properties are known to vary among different sets of observations, and variations in both time and location are observed. They are generally either unresolved or under-resolved in GCMs. The mechanisms that generate them, such as flow over topography and convection are also poorly resolved processes, so even those waves resolved in GCMs may not be realistic. The properties (e.g., horizontal and vertical wavelength and propagation direction) of a gravity wave or gravity-wave packet influences the group velocity and dissipation of the waves. Gravity waves are in turn affected by the background wind and stability of the atmosphere through which they propagate [*Lighthill*, 1978].

[4] Gravity-wave effects in GCMs are currently parameterized [*Fritts and Lu*, 1993; *Medvedev and Klaassen*, 1995; *Hines*, 1997; *Alexander and Dunkerton*, 1999; *Warner and McIntyre*, 2001]. These parameterizations require knowledge of the gravity-wave sources and details about the wave properties in the lower atmosphere to describe their effects accurately. Although each parameterization differs somewhat in its formulation, each requires specification of a gravity-wave spectrum and a launch altitude for the spectrum. This spectrum, often referred to as a ''source spectrum'' may be specified in terms of phase speed, propagation direction, frequency, and horizontal and vertical wavelengths. A measure of wave variance or momentum flux must also be specified. The spectrum may vary with time and geographic location, but is generally specified to be constant, varying only in latitude, or in the case of topographic waves, varying with topography and surface winds.

[5] There is currently insufficient information about the global properties and occurrence of gravity waves to specify gravity-wave input spectra for parameterizations. This lack of information allows far too wide a range of input parameters for the parameterizations. The lack of constraints means that the accuracy of the different parameterization methods cannot be assessed [*McLandress*, 1998; *Charron et al.*, 2002]. It also effectively provides a huge range of ''tuning parameters'' in GCM parameterization applications. Application of one parameterization in a GCM can be tuned to give realistic zonal wind fields in a certain height region or season, for example. However, these parameterization settings may have other effects not examined during the tuning procedure that may be completely unrealistic, such as altering winds at other levels or other seasons, or changing the gravity-wave/planetary-scale wave interactions.

[6] Observational constraints on the global properties and occurrence of gravity waves are therefore rather urgently needed to constrain parameterization of their effects in GCMs. Global observations of gravity waves from satellite do exist [*Fetzer and Gille*, 1994; *Wu and Waters*, 1996a, 1996b; *Preusse et al.*, 1999; *Eckermann and Preusse*, 1999]. These are measurements of temperature variance, and each emphasizes only a certain portion of the gravity-wave spectrum [*Alexander*, 1998; *Preusse et al.*, 2000]. In addition, measurements of temperature variance cannot be readily converted to momentum flux without detailed knowledge of the properties associated with every wave perturbation observed, and it is momentum flux that is needed to constrain the parameterization of gravity-wave effects in GCMs. Further, because gravity-wave sources are generally intermittent in nature, the observations tend to emphasize the waves with slower vertical group velocity, yet these are not likely associated with the largest momentum fluxes [*Alexander et al.*, 2002]. Direct observations of gravity-wave perturbations in the atmosphere therefore require additional interpretive study before they can be used to directly constrain parameterizations.

[7] In the present paper, we present a very different kind of constraint for parameterizations of gravity-wave effects. Here we present estimates of the monthly and zonal mean gravity-wave-driven momentum forcing in the stratosphere as a function of latitude, height, and time. The method was described by *Alexander and Rosenlof* [1996] and extended here to the period November 1991 to June 1997 using data from the Upper Atmosphere Research Satellite (UARS). The gravity-wave-driven force is derived by first estimating the total forcing term that must be present in the zonal mean momentum equation and then subtracting the resolved Elliassen-Palm (EP) flux divergence term leaving a residual that can be associated with smaller-scale unresolved waves plus uncertainties [*Hartmann*, 1976; *Hamilton*, 1983; *Smith and Lyjak*, 1985]. This residual force is then compared to a suite of model calculations that estimate the gravity-wave force arising from different gravity wave source spectra. Correlations are performed on specially averaged fields that emphasize important gravity-wave effects in the stratosphere: (1) forcing of the equatorial QBO and SAO oscillations and (2) forcing of the extratropical transport circulation. The results provide some constraints on differences between tropical and extratropical gravity-wave source spectra.

2. Data Analysis

[8] We derive an estimate of the zonal mean gravity-wave-driven forcing in the stratosphere from UARS data. The basic method has been described by *Alexander and Rosenlof* [1996] with some changes to the specification of radiatively active gas concentrations that are described below. The method is summarized in 2.1. The zonal mean state defined by the potential temperature $\bar{\theta}$ and zonal wind $\bar{u}$ are taken from the UK Met Office (UKMO) data set that has been output on the UARS data grid [*Swinbank and O'Neill*, 1994a]. The UKMO resolution is 3.75° longitude and 2.5° latitude with 7 vertical levels per decade of pressure. The results of our calculations are estimates of the gravity-wave-driven momentum forcing in the stratosphere as a function of latitude, pressure altitude, and time $\bar{X}(\phi, z, t)$. The top level of our analysis lies at 48.3 km (1 hPa). This is more than a scale height below the upper boundary of the UKMO assimilation in order to avoid potential boundary artifacts in our results.

2.1. Calculation of the Residual "Gravity-Wave" Forcing

[9] The transformed Eulerian mean (TEM) residual circulation ($\bar{v}^*$, $\bar{w}^*$), an approximation of the zonal mean transport circulation, is calculated by solving the TEM thermodynamic and continuity equations in spherical coor-

dinates (latitude ϕ, altitude z, time t) [*Andrews et al.*, 1987]:

$$\frac{\partial \bar{\theta}}{\partial t} + \frac{\bar{v}^*}{a}\frac{\partial \bar{\theta}}{\partial \phi} + \bar{w}^*\frac{\partial \bar{\theta}}{\partial z} = \bar{Q} \tag{1}$$

$$\frac{1}{a\cos\phi}\frac{\partial}{\partial \phi}(\bar{v}^*\cos\phi) + \frac{1}{\bar{\rho}}\frac{\partial}{\partial z}(\bar{\rho}\bar{w}^*) = 0. \tag{2}$$

The notation is standard following that in the work of *Andrews et al.* [1987] (potential temperature $\bar{\theta}$, earth radius a, density $\bar{\rho}(z)$). The flux divergence term is small under quasigeostrophic scaling, and has been ignored here. The solution technique is based on the method of characteristics, and as in the iterative method described by *Murgatroyd and Singleton* [1961], a mass balance correction is needed. Here the correction is applied along characteristic lines rather than the pressure surfaces used in *Murgatroyd and Singleton* [1961], but both techniques yield nearly the same results since the characteristic lines of the system are nearly horizontal.

[10] The calculation requires the diabatic heating rate $\bar{Q}$ as input. The radiative heating code [*Olaguer et al.*, 1992] consists of three modules. One computes solar heating, the second computes infrared (IR) heating, and a third is needed to estimate latent heating in the troposphere. The IR portion takes CO_2, O_3, H_2O, CH_4, and N_2O as inputs. The solar code calculates radiative absorption by O_3, O, and NO_2 at ultraviolet and visible wavelengths, and by H_2O and CO_2 at near-IR wavelengths. Stratospheric heating is calculated as the sum of absorption of the direct solar beam and absorption of diffuse solar radiation backscattered by the lower atmosphere. The calculation includes the effects of multiple scattering and reflection of radiation by clouds and zonal mean ground albedo (shortwave reflection), and surface temperature (longwave emission). Latent heating in the troposphere is calculated based on a global rainfall climatology. However, in the stratosphere, latent heating has no impact on the stream function solution.

[11] Inputs to the radiative heating rate calculation consist of zonally and monthly averaged ozone, water and methane from UARS measurements, UKMO temperatures [*Swinbank and O'Neill*, 1994a] and climatological values for other needed constituents and clouds. CO_2 increases linearly with time t according to globally averaged surface data collected by the Carbon Cycle Group of the National Oceanic and Atmospheric Administration (NOAA) Climate Monitoring and Diagnostics Laboratory (CMDL):

$$n_{CO_2} = n_0 + A_1 \times (t - 1973 - t_l), \tag{3}$$

where n_0 = 326.909 ppmv, A_1 = 1.50155 ppmv/year, and t_l = 2 yr (lag time for CO_2 surface values to reach the stratosphere).

[12] The calculation was done globally for the period November 1991 through June 1997. The solution ($\bar{v}^*$, $\bar{w}^*$) is then used to evaluate the total forcing term $\mathcal{F}$ in the TEM momentum equation:

$$\frac{\partial \bar{u}}{\partial t} + \bar{v}^*\left[\frac{1}{a\cos\phi}\frac{\partial}{\partial \phi}(\bar{u}\cos\phi) - f\right] + \bar{w}^*\frac{\partial \bar{u}}{\partial z} = \mathcal{F}. \tag{4}$$

[13] The total zonal momentum force is then treated as the sum of the forcing associated with the EP flux divergence ($\nabla \times \mathbf{F}$) from dissipation of all of the resolved waves in the UKMO data and the forcing associated with unresolved smaller-scale waves $\bar{X}$:

$$\mathcal{F} = \frac{1}{a\cos\phi}\nabla \times \mathbf{F} + \bar{X}. \tag{5}$$

The resolved forcing is computed from the UKMO data, subtracted from the radiatively derived total force, and the residual $\bar{X}$ is treated as an estimate of the gravity-wave-driven forcing in the stratosphere. Note that the force we derive is the east-west component of the force vector: Eastward forcing will have positive values, and westward forcing negative values.

[14] The uncertainties in this estimate of the gravity-wave forcing $\bar{X}$ are difficult to quantify, but are likely substantial. Despite the uncertainties, the transport circulation ($\bar{v}^*$, $\bar{w}^*$) and the wave forcing estimates derived via this method have withstood numerous comparisons that indicate many realistic features. The tropical upwelling $\bar{w}^*$ has been compared to estimates from tracer observations [*Mote et al.*, 1998] and used in model studies of the QBO [*Dunkerton*, 1997]. These indicated errors likely smaller than 50%. The tropical gravity-wave forcing of the QBO and SAO are also realistic in comparison to numerous analyses and global model studies [*Dunkerton*, 1997; *Giorgetta et al.*, 2002; *Jackson and Gray*, 1994]. The hemispherically averaged extratropical downward mass fluxes in the lower stratosphere derived from the transport circulation are similar to other independent estimates [*Appenzeller et al.*, 1996]. The age of air estimated from the transport circulation is also in good agreement with estimates derived from trace gas measurements.

[15] These comparisons indicate that with some averaging of the $\bar{X}$ estimates, the seasonal cycles are robust, and the magnitudes are reliable within approximately a factor of 2. We focus on two averaged latitude regions, the tropics and the extratropics.

2.2. Tropical Forcing: QBO and SAO

[16] The QBO and SAO zonal wind oscillations in the stratosphere are partly forced by gravity-wave dissipation. Gravity waves naturally aid in the descent of the phases of the QBO zonal wind oscillation through dissipation near critical levels in the lower stratosphere [*Lindzen and Holton*, 1968]. Numerous global-scale model studies have suggested that gravity waves may provide as much as half of the wave forcing required to drive the QBO (see the review by *Baldwin et al.* [2001]). We will refer to the eastward (= westerly) phases of both the QBO and SAO as "positive" wind phases, and will refer to the westward (= easterly) phases as "negative" wind phases.

[17] In the SAO, the negative phase is believed to be mainly driven by meridional advection of the summer negative winds across the equator. Dissipation of Rossby gravity waves may also contribute. The positive phase may be driven largely by Kelvin waves, though these can have a wide range of horizontal and vertical wave numbers [*Garcia and Sassi*, 1999; *Holton et al.*, 2001]. Some Kelvin waves may therefore be difficult to distinguish from eastward propagating gravity waves. Certainly, our estimates of the

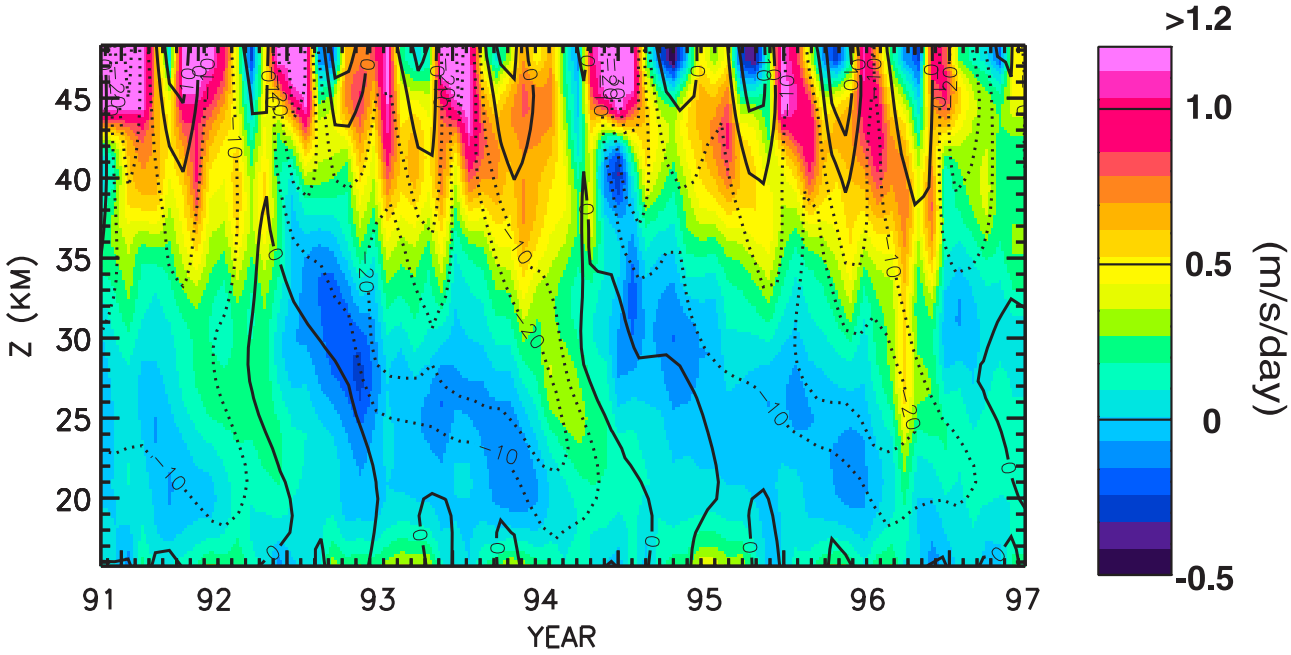

Figure 1. Color background shows the variation of $\bar{X}$ averaged over the equatorial region 15°S to 15°N as a function of time and altitude. Negative values are blue to black, positive green to pink. Peak values in the upper stratosphere SAO region are 4 m s^{-1} day^{-1}. In general, the magnitudes are expected to increase with height due to the decrease in atmospheric density. Important QBO variations occur in the lower stratosphere below ~35 km. Black contours are superimposed indicating the background winds with dashed contours representing westward winds.

gravity-wave forcing $\bar{X}$ will not distinguish between shorter-scale Kelvin waves and gravity waves.

[18] Figure 1 shows $\bar{X}$ averaged over the equatorial latitude band 15N–15S as a function of height and time. The superimposed contours show the background zonal winds. The color scale indicates values of $\bar{X}$ in m s^{-1} day^{-1}. The two most prominent features in Figure 1 are associated with the QBO and SAO: (1) below 35 km the tongues of positive force descend in time and lead the positive wind phase of the QBO and a corresponding negative force occurs during the descent of the negative QBO wind phase; (2) above 42 km, the force is nearly out of phase with the SAO wind, where positive forcing is associated with negative SAO wind phases, and a weaker negative forcing often occurs when the winds are positive. These features are better illustrated in Figure 2. The phase of $\bar{X}$ at 1 hPa (47 km) nearly matches the phase of the meridional advection term in the momentum equation (4) which is proportional to both $\bar{v}^*$ and the meridional gradient in the zonal wind. Both the meridional advection term and the net wave forcing $\mathcal{F}$ are large, while the $\partial\bar{u}/\partial t$ term is about 6 times smaller, and the other terms are negligible. If our estimates of $\bar{v}^*$ are within about a factor of 2 of reality, then the phase relationship between $\bar{X}$ and the wind at 1 hPa seen in Figure 2 is robust. $\bar{v}^*$ would need to be about 6 times too large before this is substantially affected, which is unlikely.

[19] Our estimates of the gravity-wave forcing depend sensitively on the UKMO winds shown in Figures 1 and 2. *Swinbank and O'Neill* [1994b] describe the QBO and SAO winds in these data. The oscillations have many realistic features. However, *Swinbank and O'Neill* [1994b] note that the transition from negative to positive winds in the upper stratosphere proceeds rapidly through a deep layer in the UKMO winds, in contrast to observations which show a

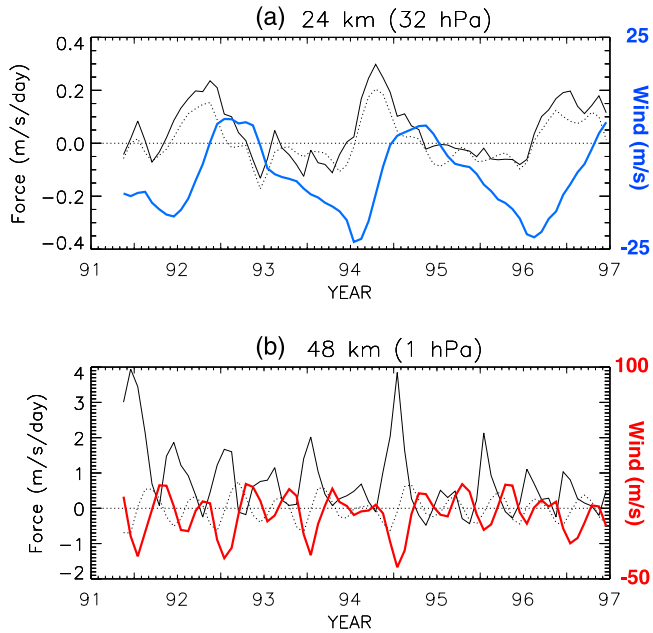

Figure 2. Gravity-wave forcing (black solid) and winds (color) (a) at 32 hPa (24 km) and (b) at 1 hPa (47 km). The dotted lines in each panel show the wind tendency $\partial\bar{u}/\partial t$.

more gradual descent of the positive wind phase at a rate of about 5 to 10 km per month. The phase of the SAO in the UKMO winds is in good agreement with *Hitchman and Leovy* [1986] at 1 hPa, and we will choose this level for our model comparisons (see section 3).

[20] It should be noted that some of the main features of the equatorial missing force $\bar{X}$ are positive (see Figure 2). We therefore reiterate that this missing force we are calling the "gravity-wave forcing" may also include smaller-scale Kelvin waves since Kelvin-wave dissipation would likewise result in a positive zonal force. Kelvin waves have the same dispersion relation as gravity waves and differ only in their meridional structure. However, observations of potential energy versus latitude for short vertical-scale waves in the tropics do not match the Kelvin-wave meridional structure suggesting a still important contribution from gravity waves [*Alexander et al.*, 2002]. The model we will describe in section 3.1 is suitable for describing smaller-scale Kelvin-wave forcing as well as gravity waves.

2.3. Extratropical Forcing: Residual Circulation and the Role of GWs

[21] The transport circulation in the stratosphere (also called the Brewer-Dobson circulation [*Brewer*, 1949]) is upward in the tropics, and poleward and downward in the extratropics. This circulation results from zonal wave-driven forces that are negative in sign. The circulation is much stronger in the winter than the summer hemisphere, and also stronger in the Northern Hemisphere winter season (December–February) than the corresponding Southern Hemisphere winter (June–August) [*Yulaeva et al.*, 1994]. These last two features are indications that the transport circulation is largely planetary wave-driven and so dominated by the EP flux divergence term $\nabla \times \mathbf{F}/(a\cos\phi)$ that we derive from the UKMO assimilation output. However, gravity waves may play a dominant role in the summer hemisphere because stationary planetary waves cannot propagate into the negative (westward) zonal winds of the summer stratosphere. Westward propagating gravity waves can propagate into the summer stratosphere, dissipate, and provide the negative (westward) force needed to drive the summer hemisphere cell of the stratospheric transport circulation [*Alexander and Rosenlof*, 1996]. The summer residual circulation, though weaker than in winter, still has a significant effect on lower stratosphere temperatures [*Rosenlof*, 1995].

[22] To examine extratropical-wave forcing effects, we evaluate the contributions of gravity-wave dissipation and resolved large-scale wave forcing to the residual circulation. To do this, we compute the density-weighted vertical integral of the forcing using the quasigeostrophic form of the downward control formula [*Haynes et al.*, 1991],

$$D(\phi) = 2\pi a \int_{z_1}^{z_T} \left[\frac{\bar{\rho}\cos\phi}{f} \times (\text{Force}) \right]_{\phi=\text{constant}} dz'. \qquad (6)$$

[23] When the "force" applied in (6) is the total momentum forcing $\mathcal{F}$, and if $z_T = \infty$, then the value of the integral is Ψ the transport circulation stream function defined by

$$\bar{v}^* = \frac{-1}{\bar{\rho}\cos\phi}\frac{\partial\Psi}{\partial z}; \quad \bar{w}^* = \frac{1}{\bar{\rho}a\cos\phi}\frac{\partial\Psi}{\partial\phi}. \qquad (7)$$

If D is evaluated at the latitude ϕ_t where $\partial\Psi/\partial\phi$ changes sign (or where $|\Psi|$ is a maximum), then $D(\phi_t)$ is the total hemispherically integrated extratropical downward mass flux across the pressure surface given by z_1. We call latitude ϕ_t the turnaround latitude [*Rosenlof*, 1995]. It is the latitude where the vertical component of the transport circulation $\bar{w}^*$ changes from positive (upward) in the tropics to negative (downward) in the extratropics.

[24] In our calculations here we let z_T = 48.3 km which is the top level of our analysis, and z_1 = 16.8 km corresponding to the 90.7 hPa pressure surface. Letting the "force" in (6) be the total wave forcing $\mathcal{F}$, then (6) gives estimates of the downward mass flux $D_{\mathcal{F}}(\phi_t)$ and the stream function in each hemisphere. We next separately substitute $\bar{X}$ and the planetary-wave forcing into (6) to compute $D_X(\phi_t)$ and $D_{EP}(\phi_t)$ respectively. These give measures of the contribution of unresolved (D_X) and resolved (D_{EP}) wave forcings to the stratospheric transport circulation total downward flux.

[25] Figure 3 shows the results of the application of (6) to the total ($D_{\mathcal{F}}$), planetary-wave-driven (D_{EP}), and gravity-wave-driven (D_X) momentum forcing terms estimated from the UARS data. The 5.5 years of data have been averaged to show the seasonal cycle. Figure 3a shows the turnaround latitudes ϕ_t for the Northern and Southern Hemispheres. Figure 3b shows the annual cycle of $D_{\mathcal{F}}(\phi_t)$ for each hemisphere. These illustrate the peak downward flux in winter in each hemisphere that is primarily associated with planetary-wave dissipation in winter D_{EP} [*Rosenlof and Holton*, 1993; *Yulaeva et al.*, 1994]. This is shown explicitly in Figures 3c and 3d where contributions from resolved and unresolved waves are plotted separately. The total $D_{\mathcal{F}}$ is dominated by D_{EP} in winter, but the gravity-wave contribution D_X dominates in the spring to summer transition season. *Alexander and Rosenlof* [1996] showed that gravity waves with westward phase speeds can provide this forcing, and the fact that GCMs commonly do not include such waves may explain the tendency for delayed springtime warming and delayed onset of the summertime westward winds in most middle atmosphere GCMs [*Hamilton et al.*, 1999]. *Scaife et al.* [2002] recently demonstrated this effect with parameterized gravity waves in a GCM.

[26] It should be emphasized that the quantities $D_{\mathcal{F}}$, D_X, and D_{EP} are poor measures of the downward mass flux during periods of rapid time changes, in particular during equinox seasons [*Rosenlof and Holton*, 1993]. The seasonal variations evident in Figure 3 are instead intended as a means of evaluating the contributions to the vertically integrated extratropical-wave forcing as a function of time. The full time series of D_X for 1991–1997 will be shown in section 3.

3. Model Comparisons

[27] We next compare $\bar{X}$ to a suite of model calculations of the gravity wave force. Each model calculation assumes a different input spectrum of gravity waves near the tropopause but uses the same background atmosphere field above as defined by the UKMO data. These model calculations are then correlated with $\bar{X}$ and the correlations give an indication of the important features of the gravity-

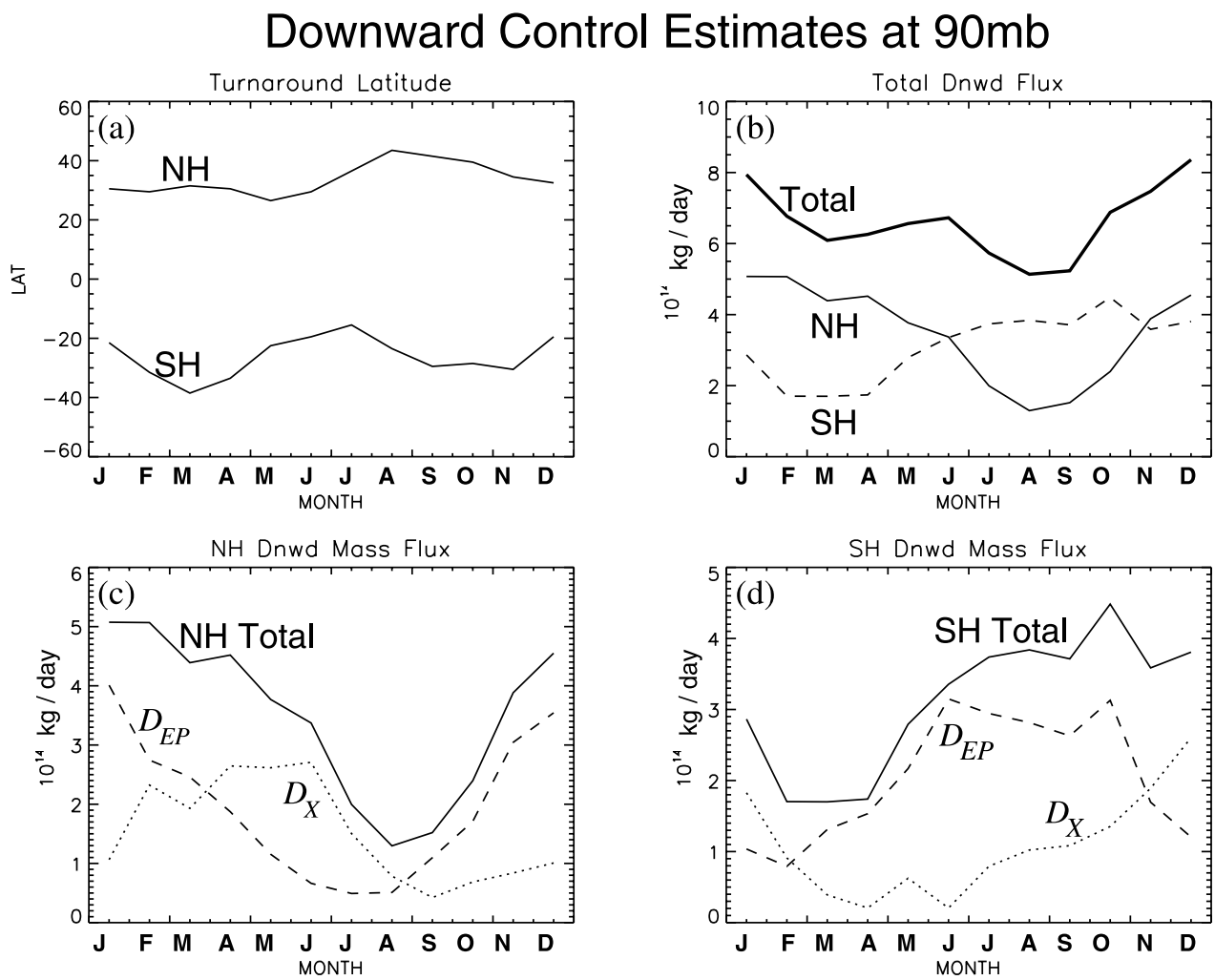

Figure 3. Estimates of the downward mass flux across the 90.7 hPa surface via (6) and contributions from gravity-wave dissipation and EP flux divergence. (a) Seasonal cycle in the turnaround latitudes (ϕ_t) where the flux $D_{\mathcal{F}}$ changes sign from upward in the tropics to downward in the extratropics (NH, Northern Hemisphere; SH, Southern Hemisphere). (b) Seasonal variation in $D_{\mathcal{F}}$ and in NH (solid) and SH (dashed). Bottom panels show contributions to $D_{\mathcal{F}}$ from EP flux divergence D_{EP} and gravity waves D_X for (c) NH and (d) SH.

wave spectrum near the tropopause that are necessary to fit the observations.

3.1. Model Description

[28] We apply a simple one dimensional model of gravity-wave propagation and dissipation, but apply it to varying background winds and stability as given by the zonal and monthly mean UKMO data on a 4.5° latitude grid. The model is the same as that applied in *Alexander and Vincent* [2000]. It uses the linear theory for gravity waves including nonhydrostatic and Coriolis effects and total internal reflection [*Alexander*, 1998] although reflection is unimportant for the range of horizontal wavelengths we consider below. The gravity waves are treated as perturbations on a locally horizontally homogeneous background atmosphere. The more important gravity wave forces in the stratosphere are zonal, so a suitable simplification we make here is to consider only zonally propagating gravity waves. The linear-wave solutions to the wind perturbations (u', v', w') are:

$$(u', v', w') = \mathrm{Re}(\tilde{u}, \tilde{v}, \tilde{w}) \exp[-(z - z_0)/2H] \exp[i(kx + mz - \omega t)] \tag{8}$$

$$\tilde{v} = -i\tilde{u}\frac{f}{\hat{\omega}}. \tag{9}$$

k and m are the horizontal and vertical wave numbers, ω the frequency in a frame of reference relative to the ground, $\hat{\omega} = \omega - \bar{u}k$, H is the density-scale height $(d(ln\bar{\rho}/dz)^{-1})$, z_0 is a reference altitude for the wave amplitudes, and f is the Coriolis parameter. These solutions are exponentially growing with height, but the amplitude growth is limited in the model by a saturation condition given by the

convective instability criterion that can be written as [*Dewan and Good*, 1986],

$$|w'| \leq \left|\frac{\hat{\omega}}{m}\right|. \tag{10}$$

If wave amplitudes try to grow larger than this limit, the model assumes enough wave dissipation to reduce the amplitude back to this limit. This saturation model roughly reproduces the wave energy spectrum proportional to m^{-3} observed in the middle atmosphere [*Alexander*, 1996].

[29] The dispersion relation gives the relationship between the intrinsic frequency $\hat{\omega}$ and the horizontal and vertical wave numbers k and m:

$$\hat{\omega} = \frac{N^2k^2 + f^2(m^2 + \alpha^2)}{k^2 + m^2 + \alpha^2}. \tag{11}$$

The term f varies with latitude and $\alpha = 1/(2H)$ and $N^2 = g\partial(\ln\theta)/\partial z$ (buoyancy frequency) vary with both height and latitude. The intrinsic frequency $\hat{\omega}$ will vary as the zonal wind $\bar{u}$ varies with height,

$$\hat{\omega} = \omega - k\bar{u}. \tag{12}$$

In this one-dimensional model, the effects of horizontal variations in the background atmosphere are neglected in the dynamical equations, so k and ω remain constant with height. In the absence of dissipation, the momentum flux $\bar{\rho}\overline{u'w'}$ is also constant in height. The gravity-wave-driven force is given by

$$\bar{X}_M = -\frac{1}{\bar{\rho}}\frac{\partial}{\partial z}\left(\bar{\rho}\overline{u'w'}\right), \tag{13}$$

which is only nonzero where there is dissipation.

[30] The above equations treat the propagation and dissipation of a monochromatic wave (one with single values of k, ω, and m defined at z_0). We treat a spectrum of waves as the linear sum of monochromatic waves. The momentum flux and the net force are both computed as the sum over all the waves in the spectrum, e.g.,

$$\text{total flux} = \epsilon\bar{\rho}\sum_c \overline{u'w'}, \tag{14}$$

where ϵ is an intermittency factor (generally $\ll 1$) that crudely takes into account the spatial and temporal intermittency in wave activity within a monthly mean latitude band. It will be chosen as a constant in latitude and time for each model run, but will vary among the different model runs.

Table 1. Model Gravity-Wave Parameters

Parameter	Description	Range of Values
$\bar{\rho}\overline{u'w'}$	source spectrum shape	equations (15) and (16)
c_w	source spectrum width	5 to 80 ms^{-1}
k	horizontal wave number	$2\pi/100$ to $2\pi/4000$ km
B_m	spectrum amplitude	1 to 10 $m^2\ s^{-2}$
z_0	source altitude	15.75 km

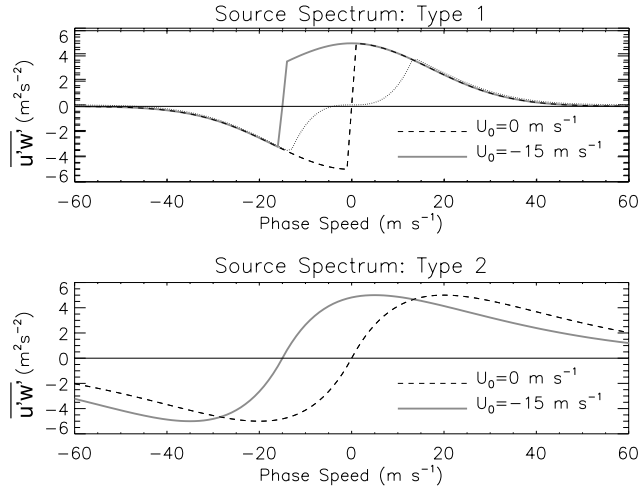

Figure 4. Examples of type 1 (15) and type 2 (16) gravity wave source amplitude spectra $\overline{u'w'}$ versus ground-based phase speed c. The gray lines show the result for source level wind $U_0 = -15$ m s^{-1} and the dashed lines for $U_0 = 0$. The dotted line in the top panel shows how the dashed line spectrum is modified at the source level by the saturation condition (for $\lambda_x = 2\pi/k = 100$ km).

[31] This model is most similar to current applications of the *Lindzen* [1981] parameterization that is still widely used in GCMs, so the results should be most suitable for constraining Lindzen-type gravity-wave parameterizations. Our model differs from other spectral parameterizations in either the dissipation mechanism or the treatment of the spectrum, but the one-dimensional wave propagation approach is common to all parameterizations of gravity-wave effects used in GCMs. The conclusions we draw in section 5 are general enough that they will also help to constrain other parameterizations. We will discuss some of these issues further in section 4.

3.2. Input Spectra

[32] The "source spectrum," input at level z_0, is allowed to vary with a wide range of parameters given in Table 1. The spectral shapes that result are illustrated with examples shown in Figure 4. Two basic types of input gravity wave momentum flux amplitude spectra $\overline{u'w'}$ are examined. Type 1 always peaks at a ground-based phase speed $c = 0$:

$$\overline{u'w'} = \pm B_m \exp\left[-\left(\frac{c}{c_w}\right)^2 \ln 2\right]. \tag{15}$$

Type 2 is instead symmetric about the phase speed $c = \bar{u}_0$, the wind speed at the source level $\bar{u}_0 = \bar{u}(z_0)$:

$$\overline{u'w'} = B_m\left(\frac{c - \bar{u}_0}{c_w}\right)\exp\left[1 - \frac{|c - \bar{u}_0|}{c_w}\right]. \tag{16}$$

The parameter c_w determines the width of the spectral distribution as a function of phase speed, and B_m determines the wave amplitudes. A horizontal wave number k is also chosen, and specified as a constant across all phase speeds in the spectrum, but k is allowed to vary among different

model runs. The wind at the source level $\bar{u}_0$ varies with latitude and time in accordance with the UKMO data, so despite constant parameters c_w, B_m, and k, the input spectrum will vary with the value of $\bar{u}_0$ as illustrated in Figure 4. We truncate the spectra at ±60 m s^{-1} phase speeds, expecting that higher phase speeds are less important in the stratosphere than in the mesosphere. Consequently, our results in the stratosphere are not expected to adequately constrain the properties of very high phase-speed waves. We fix z_0 = 15.75 km since most GCM applications specify nonstationary waves near the tropopause.

[33] This method of specifying the wave spectrum input to the model is oversimplified compared to the likely real gravity-wave spectrum present in the atmosphere. However, the parameters chosen are similar to those that need to be specified in many GCM gravity wave parameterizations, and the range of parameters allows an exploration of the sensitivity of the gravity-wave forcing to some of these largely unconstrained input variables.

[34] It should be noted that the input spectrum as it has been specified may contain some unstable waves, so their amplitudes will be trimmed at the input altitude before the wave propagation with height and mean flow forcing calculation begins. This will tend to be true for waves with very small intrinsic phase speeds $|\hat{c}| = |c - \bar{u}_0|$ and some waves with the largest input amplitudes (near the peaks in the spectra with large B_m). The most extreme case would be a type 1 spectrum with large B_m and small $\bar{u}_0$. Figure 4 also illustrates how this spectrum would be trimmed at the source level by the saturation condition (10).

[35] We will be correlating modeled and observed gravity-wave forcing diagnostics using linear correlation [*Bevington and Robinson*, 1992] in time. Correlation coefficients r are deemed significant when

$$1 - \mathrm{erf}\left(\frac{r\sqrt{N}}{\sqrt{2}}\right) \leq 0.1, \tag{17}$$

where N is the number of elements in the correlation.

3.3. Tropical Forcing Parameter Study

[36] A total of 240 combinations were run to explore the range of input parameters described in Table 1. The model is run as a function of latitude, time, and height for a given set of input variables B_m, c_w, and k. The output is gravity-wave mean flow forcing $\bar{X}_M$ that is subsequently compared to $\bar{X}$ derived from the observations. To compare these, we first take the latitudinal average from 15°S to 15°N which isolates the forcing symmetric about the equator. We then compute the correlation in time between the modeled and observed equatorial forcing as a function of height. Figures 5 and 6 show maps of these correlation coefficients at two heights, 24 km and 48 km, to focus on altitudes where the QBO and SAO signals dominate respectively. The shaded regions in each map indicate where the correlations are significant. Each map shows r as a function of horizontal wavelength $\lambda_x = 2\pi/k$ and c_w for a different value of B_m. In each of these cases z_0 = 15.75 km and the type 2 source spectrum shape given by (16) was specified. These gave the best fits, although z_0 = 17.85 km and source function (15) were also explored and gave broadly similar results. With different input choices like these, the specific best fit values of wave amplitude, input flux and phase-speed width parameter change, but the shapes of the correlation maps (Figures 5 and 6) and our conclusions do not change.

[37] In Figure 5, all of the model calculations are significantly correlated with the observations, indicating that the pattern of time variations in the QBO forcing is not very sensitive to the gravity-wave spectrum input parameters. The features of the forcing that have the greatest effect on the correlation are the sharp peaks in eastward forcing that occur during the descent of the positive wind phase of the QBO (see Figure 2a). These occur naturally in the strong shear zones where gravity waves dissipate as they approach critical levels (where the phase speed of the wave approaches the wind speed $c - \bar{u}(z) \rightarrow 0$). The models reproduce this feature as long as waves with eastward momentum flux and with phase speeds in the range ~±20 m s^{-1} are input in the wave spectrum. Although the full parameter space shows significantly high correlation coefficients in time in the lower stratosphere at QBO altitudes, the slope and intercept of the linear regression further describe how well the model captures both the brief, large magnitude positive forcing peaks as well as the longer-duration, lower magnitude negative forcing in the observed time series (Figure 2a). These features are best modeled with the parameter choices in the region outlined by the dashed line in Figure 5d. These additional conditions on the slope and intercept primarily constrain the properties of the negative phase-speed (westward propagating) gravity waves.

[38] In contrast to the lower stratosphere data and model comparison, Figure 6 shows that only a more limited range of wave input parameters give high correlation coefficients in the upper stratosphere where the gravity forcing is dominated by SAO variations. Many parameter combinations in fact result in anticorrelation between data and model in the upper stratosphere (regions of negative correlation). In addition, only a more limited region of the parameter space gives reasonable forcing magnitudes, within a factor of 2. The upper stratosphere forcing is best modeled with wide phase-speed spectra $c_w > 40$ m s^{-1}, small B_m = 1 m^2 s^{-2}, and large λ_x = 4000 km. Similar results can also be obtained with larger B_m if the horizontal wavelength is simultaneously chosen to be smaller. This is generally true for linearized wave propagation models like this because smaller horizontal wavelengths tend to break at higher altitudes than larger horizontal wavelengths, and the same trend is true for wave amplitudes (i.e., smaller amplitudes break at higher altitudes than larger amplitudes). These regions of parameter space are outlined by the dashed lines in Figures 6a–6d, and mainly constrain the positive phase speed (eastward propagating) gravity waves.

[39] The best correlations for each altitude region are described in Table 2, as well as one of the best overall fits to both regions. The best overall fit is obtained with different input parameters for the positive and negative phase-speed waves (eastward and westward propagating, respectively): The negative phase-speed waves are assigned the properties shown by the circle in Figure 5d, and the positive phase-speed waves by the circle in Figure 6a. This case with asymmetric properties for the positive and negative phase-speed waves is also described in Table 2. Figure 7 compares

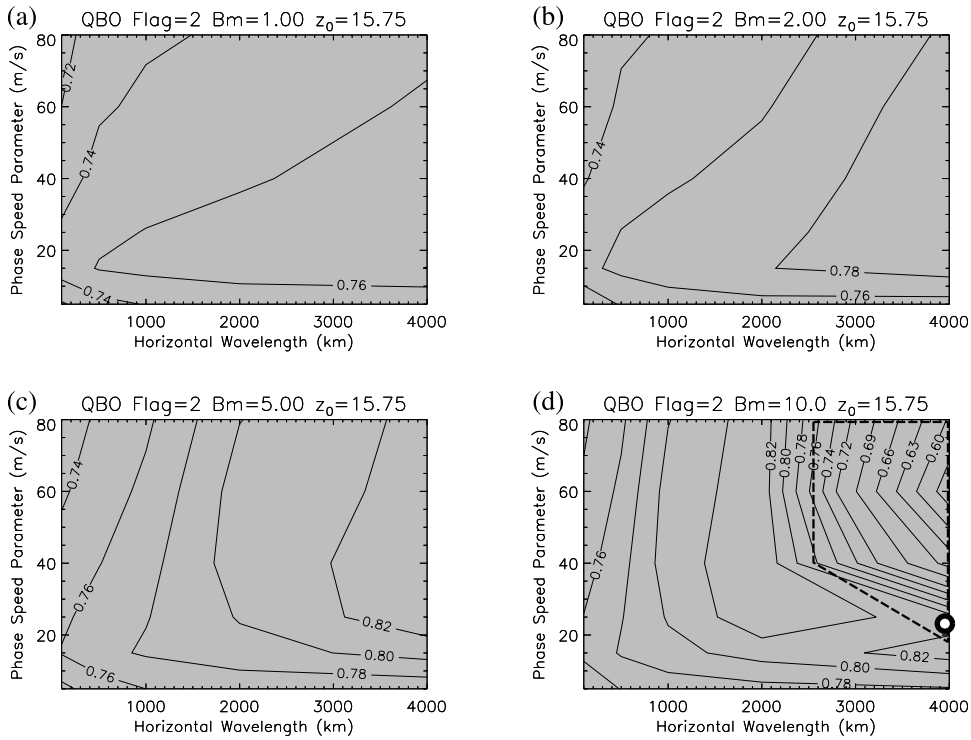

Figure 5. Results of the linear correlations between observed and modeled gravity-wave forcing time series at 24 km altitude. Each map shows correlation coefficient r versus horizontal wavelength and phase -speed width parameter c_w. (a)–(d) Results for four different spectrum amplitude parameters B_m. The background shading indicates that all regions of the parameter space give significant time correlations. Inside the region outlined with a dashed line is where the correlation slope ~1 and the intercept ~0. The circle marks the properties chosen for westward propagating waves for the special case described in the text.

the observed $\bar{X}$ to the modeled $\bar{X}_M$ for this case, and Figure 8 illustrates the best fit input spectra.

[40] In general, these results suggest that the tropical gravity waves driving the QBO and SAO in the stratosphere have large horizontal wavelengths. It also suggests the eastward and westward propagating waves likely have different properties: (a) The westward propagating waves have large horizontal wavelengths (~ thousands of km) and large amplitudes so that they become unstable in the lower stratosphere. The net westward flux entering the stratosphere is ~−.0005 Pa on average. (b) The eastward propagating waves have either large horizontal wavelength and smaller amplitude, or they have smaller horizontal wavelength and similar amplitude to the westward waves. The eastward wave spectrum also has a significantly broader distribution of phase speeds. These properties insure that the eastward propagating waves break at higher altitudes than their westward propagating counterparts. The net eastward flux entering the stratosphere is similar ~+0.0004 Pa on average.

3.4. Extratropical Forcing Parameter Study

[41] A similar model parameter exploration study was performed at extratropical latitudes. The observed and modeled time series of D_X were correlated, and the resulting correlation coefficients are shown in Figure 9 for the Northern and Southern Hemispheres separately. Both the observed and modeled D_X are evaluated at the same ϕ_t shown in Figure 3a. The better fits are obtained using the source spectrum described by (15) that always peaks at $c = 0$. Since extratropical winds at the z_0 = 15.75 km input level are generally positive (eastward), this source results in an asymmetric flux spectrum with excess negative (westward) momentum flux.

[42] As before, the shaded areas in Figure 9 show regions where the correlations are significant. Some of the regions of the parameter space result in negative correlations where the seasonal variation in the modeled and observed D_X are approaching opposite phase. The parameter set that gives the best overall fit in both hemispheres has the shortest horizontal wavelength considered, small amplitudes, and moderate phase-speed spectral widths (see Table 3).

[43] The results are strikingly different from the tropical gravity-wave study, which instead favored much longer horizontal wavelengths, and larger amplitudes. The "best fit" model (Table 3) is compared to the observed $D_X(\phi_t)$ in Figure 10. This "best fit" model gives an approximately correct seasonal cycle and a good fit to the important summertime values (section 2.3), but it results in large negative values of D_X in the winter season that do not appear in the observations. These large negative winter values in the model would suggest a gravity-wave contribution to the extratropical mass flux that is upward, opposite in sign to the planetary-wave contribution to the winter mass flux, and opposite in sign to the total observed mass flux. The observed D_X in winter is opposite showing

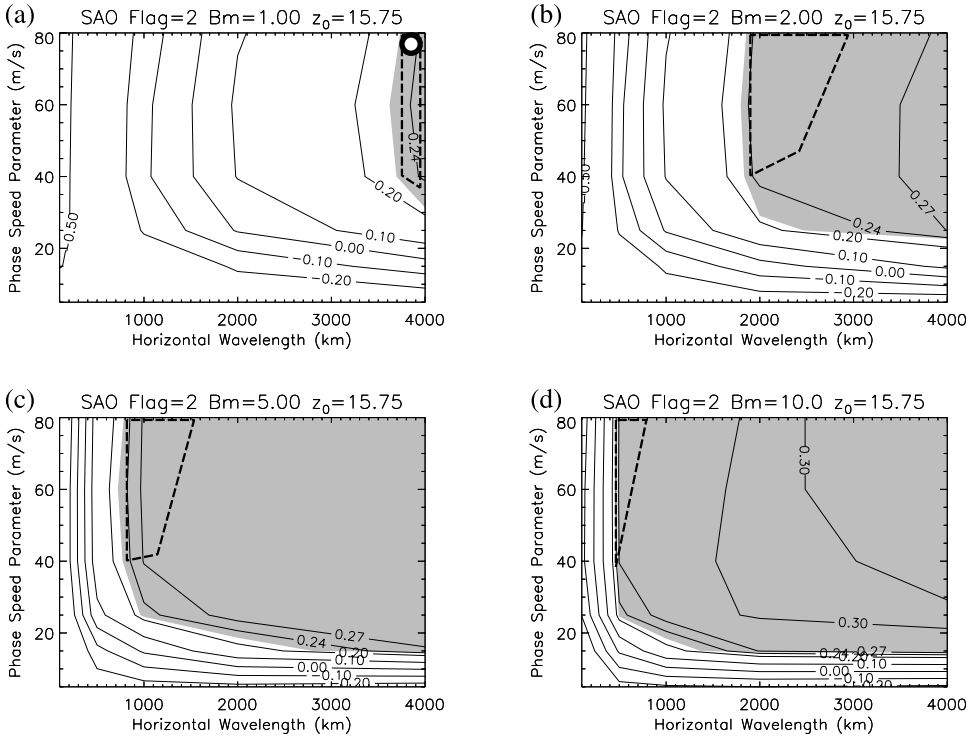

Figure 6. Results of the linear correlations between observed and modeled gravity-wave forcing time series at 48 km altitude. Each map shows correlation coefficient r versus horizontal wavelength and phase -speed width parameter c_w. (a)–(d) Results for four different spectrum amplitude parameters B_m. The background shading indicates regions of the parameter space with significant time correlations. Regions outlined by the dashed lines show where the correlation slope ~1–2 and the intercept is small. The circle marks the properties chosen for eastward propagating waves for the special case described in the text.

instead a weak but mainly positive contribution from gravity waves to the total downward mass flux.

[44] To better reproduce the seasonal cycle in the gravity-wave contribution to extratropical downward mass flux, the fall-to-winter season gravity-wave input spectrum was assigned a narrower range of phase speeds than the spring-to-summer gravity wave input spectrum. This modified seasonal cycle is also described in Table 3 and shown in Figure 11. A broad phase-speed spectrum in summer would be expected if convection were a dominant source for gravity waves, and a narrower phase-speed spectrum would be expected in winter if orographic gravity waves were much more important. We have not separately re-explored the full parameter space allowing each of the spectrum input parameters to change with season because the uncertainty in the observed D_X is probably too large to warrant such a detailed fit. However, this simple seasonal change in the phase speeds of the waves dramatically improves the modeled seasonal cycle and is supported by our knowledge of the properties of gravity waves from different sources and their seasonal cycle. We will further describe observational evidence that supports the conclusions of this study in section 4.

4. Summary and Discussion

[45] We computed unresolved zonal wave forcing in the stratosphere from UARS and UKMO data as a function of latitude, height and time. The results represent the missing wave forcing that most global models must obtain via a

Table 2. Tropical Best Fit Parameters[a]

Case	QBO, 32 hPa Best Fit	SAO, 1 hPa Best Fit	Overall Tropics	
			Westward	Eastward
$\bar{\rho}_0\overline{u'w'}$	equation (16)	equation (16)	equation (16)	equation (16)
c_w, ms^{-1}	25	80	25	80
$2\pi/k$, km	4000	4000	4000	4000
B_m, m^2 s^{-2}	10	1	10	1
Mean flux across the tropopause, Pa	±0.0005	±0.0004	−.0005	+.0004
Linear correlation, hPa	32	1	32	1
Coefficient	0.84	0.25	0.86	0.31

[a]These specific values will be model- and parameterization-dependent.

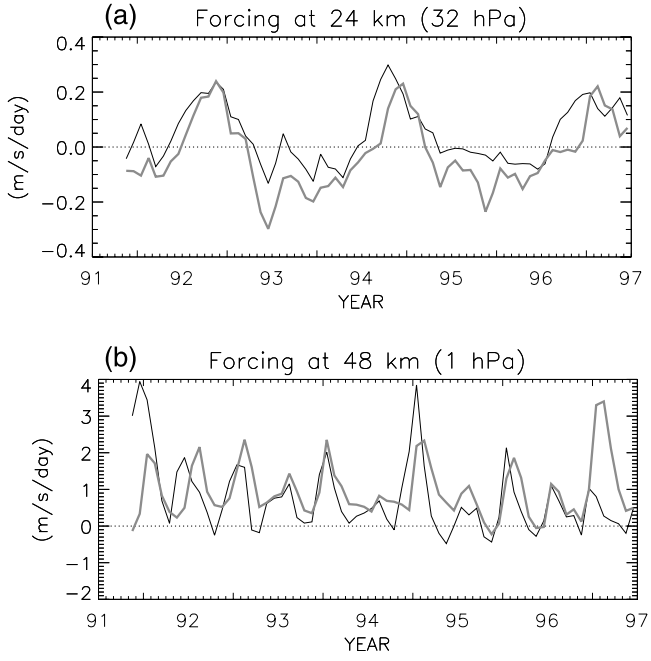

Figure 7. Best fit model with the asymmetric source spectrum described in Table 2 at (a) lower stratosphere (QBO) and (b) upper stratosphere (SAO) altitudes. The black line shows the observed $\bar{X}$ and the gray lines show the model $\bar{X}_M$.

gravity-wave parameterization. We next applied a simple model of gravity-wave propagation and dissipation to compute gravity-wave forcing for comparison to the observed forcing. Our simple model is similar to what is commonly called the Lindzen gravity-wave parameterization, but with added effects of the Coriolis force and back reflection. Our model also includes a more detailed description of the gravity wave spectrum input near the tropopause than is commonly applied with the Lindzen parameterization. With this simple model, we explored a broad range of gravity-wave input spectrum parameters and search for constraints on this input spectrum required to generate a modeled forcing that matched key features of the observed forcing. The deduced input spectrum characteristics should provide some useful constraints for applications of gravity-wave parameterizations in global models. The results suggested very different gravity-wave properties in tropical and extratropical regions and an important seasonal variation in the extratropics.

[46] In the tropics, the results indicated large gravity-wave horizontal wavelengths of several thousand km for the westward propagating waves and at least 500 km for the eastward propagating waves. Similar large horizontal wavelengths were deduced for gravity waves observed in tropical radiosonde data [*Vincent and Alexander*, 2000; *Alexander and Vincent*, 2000] and CRISTA measurements in the lower stratosphere (P. Preusse et al., personal communication, 2003) supporting the existence of such waves in the tropics. Both our estimates of $\bar{X}$ and these gravity-wave observations likely include some blend of ordinary gravity waves and equatorially trapped wave modes that have horizontal or vertical wavelengths too small to appear in the UKMO wind and temperature fields [e.g., *Holton et al.*, 2001; *Wada et al.*, 1999; *Sato and Dunkerton*, 1997; *Vial et al.*, 2001; *Hertzog et al.*, 2002]. Our analysis suggests phase speeds for these tropical waves cover a broad range and high phase speeds of $\sim$40–60 m s^{-1} appear to be very important. Gravity waves observed by the MLS on UARS at $\sim$15° latitude were inferred to have high phase speeds and were highly correlated with deep convective clouds [*McLandress et al.*, 2000], although these measurements in particular focused on mainly shorter horizontal wavelength waves. Deep convection is a likely source for high phase-speed waves because deep convective heating is associated with fast horizontal phase speeds [*Alexander et al.*, 1995; *Holton et al.*, 2002; *Beres et al.*, 2002]. *Alexander and Vincent* [2000] also inferred convection as the likely source for low phase-speed waves observed during high tropopause zonal wind conditions. Several other observational studies have also inferred convection as a source for tropical gravity waves [e.g., *Larsen et al.*, 1982; *Pfister et al.*, 1993; *Allen and Vincent*, 1995; *Dewan et al.*, 1998; *Tsuda et al.*, 2000; *Alexander et al.*, 2000]. Both eastward and westward propagating waves are important to the tropical stratospheric forcing, although at different heights. Both are important in the lower stratosphere (QBO region), and eastward waves are more important in the upper stratosphere (SAO region). These results are broadly consistent with previous studies of the role of gravity waves in the QBO and SAO [e.g., *Takahashi and Boville*, 1992; *Jackson and Gray*, 1994; *Dunkerton*, 1997; *Sassi and Garcia*, 1997; *Ray et al.*, 1998] although other details of the wave properties differ in these studies, as well as the magnitude of the gravity-wave momentum fluxes. For SAO studies, these differences are not surprising since most do not include a QBO wind oscillation in the lower stratosphere, which would substan-

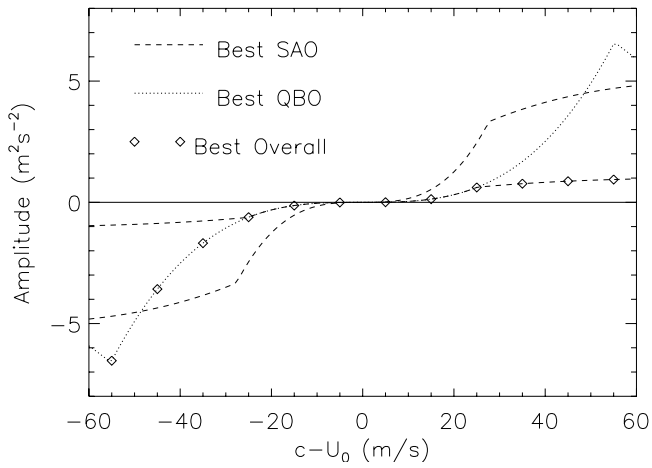

Figure 8. Amplitude spectra $\left(\overline{u'w'}\right)$ for the waves entering the stratosphere in the best fit model cases described in Table 2 and the text. The range of upper stratosphere (SAO) cases are shown with dashed lines: The case with larger amplitudes has λ_x = 1000 km, and the case with smaller amplitudes has λ_x = 4000 km. Both cases have net fluxes of ±0.0004 Pa implying more intermittent wave forcing for the larger amplitude case. The dotted line shows the best fit in the lower stratosphere (QBO), and the symbols show the asymmetric case that best fits both regions.

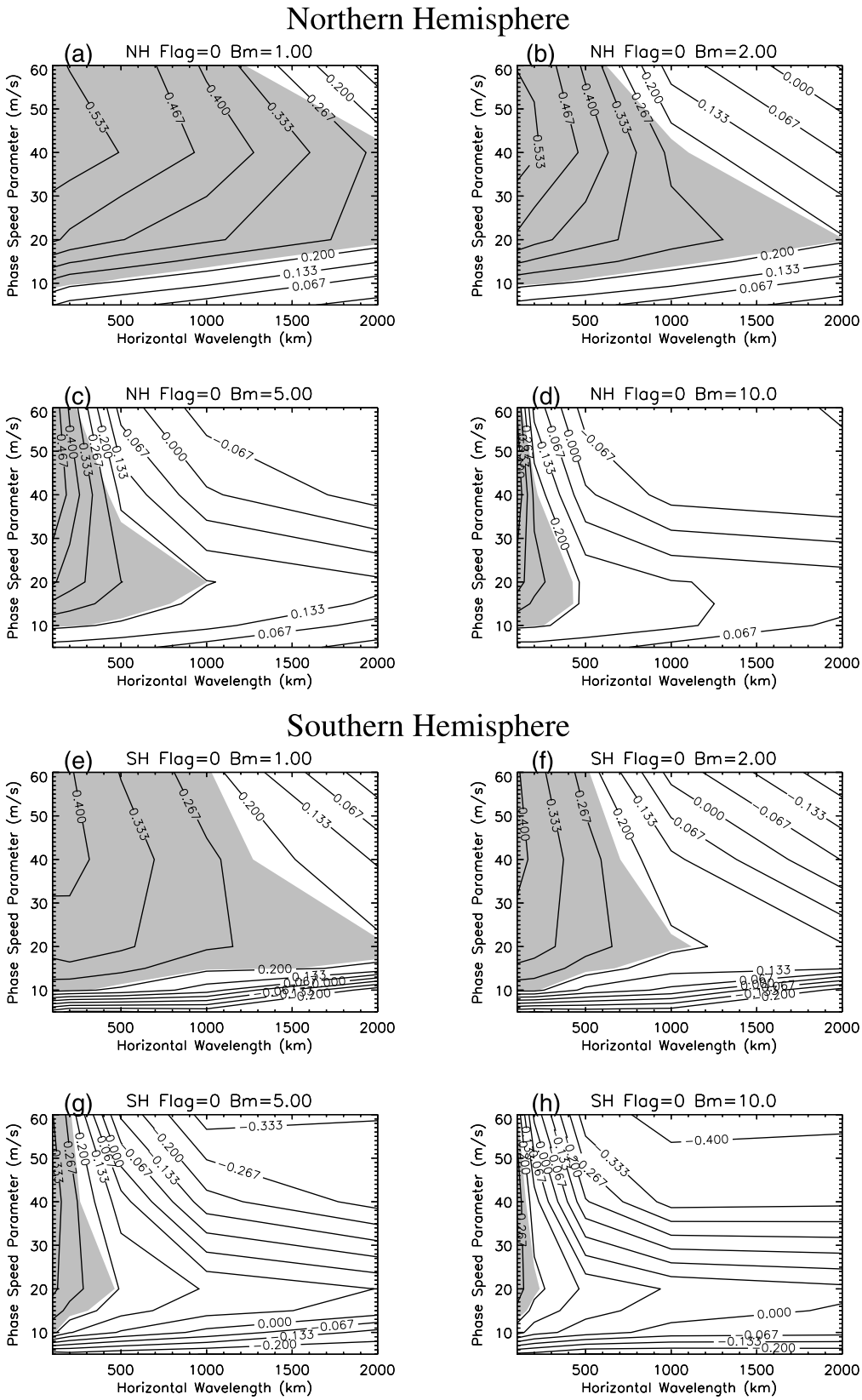

Figure 9. Correlations between the modeled and observed time series of D_X for (a)–(d) the Northern Hemisphere and (e)–(g) the Southern Hemisphere. The panels show correlation coefficients as functions of horizontal wavelength and phase-speed width parameter (c_w) for four different peak spectrum amplitudes (B_m) as marked. The shaded regions are significant according to (17).

Table 3. Extratropical Best Fit Parameters[a]

Case	Single Parameter Set Best Fit	Seasonal Variation Best Fit
$\bar{\rho}_0\overline{u'w'}$	equation (15)	equation (15)
c_w, ms^{-1}	40	40 (summer) 5 (winter)
$2\pi/k$, km	100	100
B_m, m^2 s^{-2}	1	1
Mean flux across the tropopause, Pa	0.0014 (SH) 0.0013 (NH)	0.0015 (SH) 0.0014 (NH)
Linear correlation coefficient	SH = 0.43 NH = 0.58	SH = 0.48 NH = 0.45

[a]These specific values will be model- and parameterization-dependent.

tially alter the gravity-wave propagation and dissipation through the stratosphere.

[47] In the extratropics, the results of the model comparison suggest much smaller horizontal wavelengths and a somewhat narrower range of phase speeds than in the tropics. There is an emphasis on westward momentum flux associated with the preference for the type I spectrum and the predominately eastward tropopause winds in the extratropics. An important seasonal variation in the wave spectrum is also evident, with a broader range of phase speeds in spring/summer and a much narrower range of phase speeds in fall/winter. This seasonal shift in phase speeds is consistent with more emphasis on convective sources in the spring/summer and orographic sources in the fall/winter. High-phase-speed waves were seen in the extratropical summer season in MLS data associated with deep convection in central North America [*McLandress et al.*, 2000]. Other studies have also inferred convection as the source of gravity waves observed in the summertime at extratropical latitudes [*Sato*, 1992; *Sato et al.*, 1995]. Orography has also been inferred as the source for gravity waves observed in the extratropical stratosphere in winter in numerous observational studies [e.g., *Sato*, 1994; *Whiteway et al.*, 1997; *Worthington*, 1999] and in both fall and spring in the lower stratosphere by *Eckermann and Preusse* [1999].

[48] The basic conclusions we outline here are likely to be robust irrespective of the gravity-wave parameterization that is applied whereas the details of the "best fit" spectrum at the input level will no doubt change from one application to the next. For example, using the *Alexander and Dunkerton* [1999] parameterization instead of a Lindzen-type saturation mechanisms would likely require smaller wave amplitudes than given in Tables 1 and 2. The input fluxes could also vary dramatically from those we list. For example, many of the waves in the tropical spectrum may be deleted at the input level from the *Alexander and Dunkerton* [1999] parameterization because their amplitudes will be unstable. So much larger fluxes might need to be specified to get similar fluxes propagating into the stratosphere. Other parameterizations may not be as flexible in the choice of input parameters, so these might instead require approximations that simply give similar effects.

[49] We also note that although the "best fit" solutions to both the tropical and extratropical studies tended to be at the limits of the range of parameters we considered, we do not think it is valuable to extend this range for a variety of reasons. Shorter horizontal wavelength solutions would get into the issue of back-reflection of waves, but back-reflection is handled differently in different GCM parameterization applications. Most neglect the process. Longer horizontal wavelengths become unrealistic to parameterize because parameterizations assume that the gravity waves in each GCM grid box are independent of their neighbors. Choosing a higher phase-speed width parameter over the ±60 m s^{-1} range of phase speeds we consider would serve only to produce a slightly more flat spectrum, so the solutions would be similar to those we examined.

[50] Rather than exploring the range of parameters further, it is wiser to simply take the solutions as broad indicators of general wave characteristics, e.g., short versus long wavelengths, fast versus slow phase speeds, etc.

5. Conclusions

[51] The uncertainties in our calculations are large, but some general distinguishing properties of the "missing force" emerge and some differences between tropical and extratropical gravity waves are clear.

[52] 1. The tropical gravity-wave forcing shows both QBO and SAO variations (Figures 1 and 2; section 2.2). Our model of gravity-wave forcing in the tropics reproduces similar QBO and SAO variations without any temporal variations in the input gravity-wave spectrum if the input waves have certain characteristics.

[53] 2. The gravity waves that generate the tropical forcing have long horizontal wavelengths (∼500 km or larger) and a relatively broad range of phase speeds (Figures 5 and 6). Important differences between the eastward and westward propagating waves are implicated (Table 2; Figure 7; section 3.3). The best solutions tend to favor a broader (flatter) phase-speed spectrum for the eastward propagating waves. Most current applications of

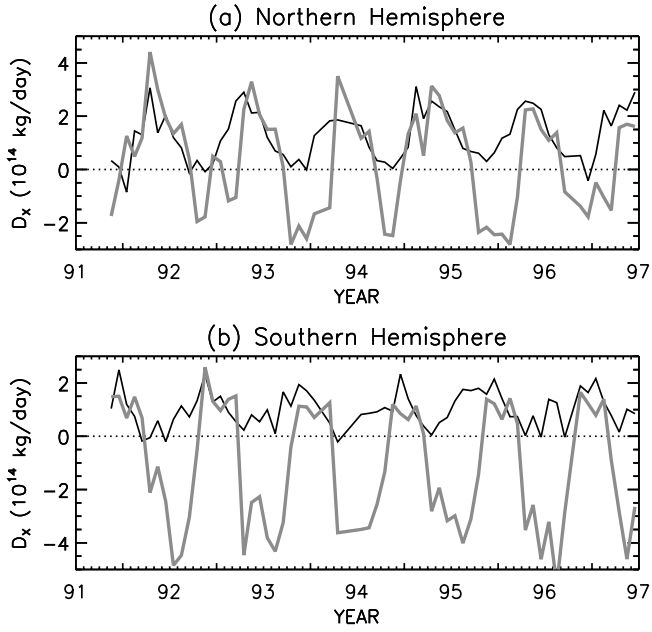

Figure 10. "Best fit" model for $D_X(\phi_t)$ (gray) compared to observed (black) for (a) the Northern Hemisphere and (b) the Southern Hemisphere. The parameter set for this model is λ_x = 100 km, c_w = 40 m s^{-1}, and B_m = 1 m^2 s^{-2}.

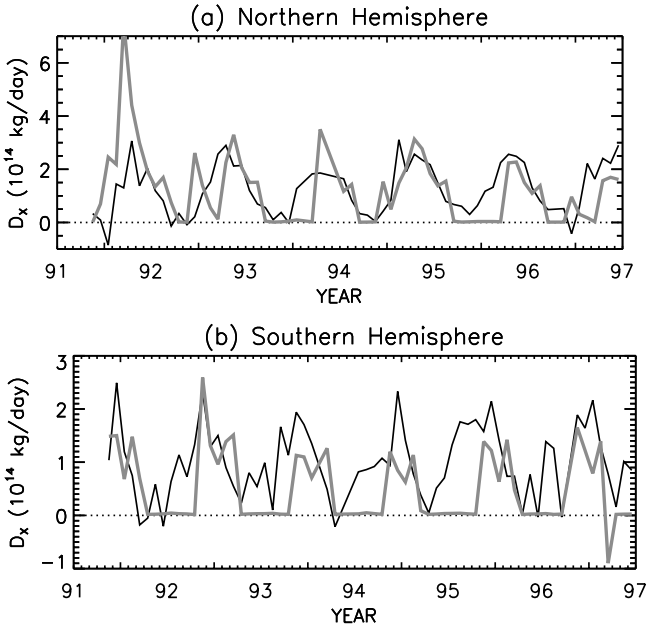

Figure 11. Another model for $D_X(\phi_t)$ (gray) compared to observed (black) for (a) the Northern Hemisphere (NH) and (b) the Southern Hemisphere (SH). The parameter set for this model includes a seasonal variation in the width of the phase-speed spectrum: $\lambda_x = 100$ km, $c_w = 40$ m s^{-1} (spring-summer), $c_w = 5$ m s^{-1} (fall-winter), and $B_m = 1$ m^2 s^{-2}. For the NH, spring-summer is defined as April–August and fall-winter as September–March. For the SH, spring-summer is November–March, and fall-winter is April–October.

gravity-wave parameterizations specify smaller horizontal wavelengths and no differences in the properties of eastward and westward propagating waves.

[54] 3. Extratropical gravity waves have important contributions to driving the springtime transition to negative (westward) stratospheric winds and to driving the summer hemisphere cell of the transport circulation (Figure 3; section 2.3).

[55] 4. The gravity waves responsible for the extratropical forcing have generally short horizontal wavelengths ~100 km (Table 3; Figure 9), and an excess of westward momentum flux (opposite to the tropopause winds) is indicated.

[56] 5. Important seasonal variations in the extratropical gravity-wave phase speeds are implicated: Higher phase speeds in spring and summer; Phase speeds much closer to zero (~ stationary waves) in fall and winter (Table 3; Figures 10 and 11; section 3.4).

[57] 6. This seasonal variation in phase speed is consistent with important convective sources in spring/summer, switching to more important orographic sources in fall/winter. Most current applications of gravity-wave parameterizations use similar small horizontal wavelengths, but they either treat only orographic waves, or if nonstationary waves are included, no seasonal variation is imposed.

[58] **Acknowledgments.** This work was supported by NASA Atmospheric Chemistry Modeling and Analysis Program grant NASW-01017. We would like to thank Elisa Manzini, Chris Meyer, and Wei Tan, as well as two anonymous reviewers, for valuable comments.

References

Alexander, M., A simulated spectrum of convectively generated gravity waves: Propagation from the tropopause to the mesopause and effects on the middle atmosphere, *J. Geophys. Res.*, *101*, 1571–1588, 1996.

Alexander, M., Interpretations of observed climatological patterns in stratospheric gravity wave variance, *J. Geophys. Res.*, *103*, 8627–8640, 1998.

Alexander, M., and T. Dunkerton, A spectral parameterization of mean-flow forcing due to breaking gravity waves, *J. Atmos. Sci.*, *56*, 4167–4182, 1999.

Alexander, M., and K. Rosenlof, Nonstationary gravity wave forcing of the stratospheric zonal mean wind, *J. Geophys. Res.*, *101*, 23,465–23,474, 1996.

Alexander, M., and R. Vincent, Gravity waves in the tropical lower stratosphere: A model study of seasonal and interannual variability, *J. Geophys. Res.*, *105*, 17,983–17,993, 2000.

Alexander, M., J. Holton, and D. Durran, The gravity wave response above deep convection in a squall line simulation, *J. Atmos. Sci.*, *52*, 2212–2226, 1995.

Alexander, M., J. Beres, and L. Pfister, Tropical stratospheric gravity wave activity and relationship to clouds, *J. Geophys. Res.*, *105*, 22,299–22,309, 2000.

Alexander, M., T. Tsuda, and R. Vincent, On the latitudinal variations observed in gravity waves with short vertical wavelengths, *J. Atmos. Sci.*, *59*, 1394–1404, 2002.

Allen, S., and R. Vincent, Gravity wave activity in the lower atmosphere: Seasonal and latitudinal variations, *J. Geophys. Res.*, *100*, 1327–1350, 1995.

Andrews, D., J. Holton, and C. Leovy, *Middle Atmosphere Dynamics*, Academic, San Diego, Calif., 1987.

Appenzeller, C., J. Holton, and K. Rosenlof, Seasonal variation of mass transport across the tropopause, *J. Geophys. Res.*, *101*, 15,071–15,078, 1996.

Bacmeister, J. T., Mountain-wave drag in the stratosphere and mesosphere inferred from observed winds and a simple mountain-wave parameterization scheme, *J. Atmos. Sci.*, *50*, 377–399, 1993.

Baldwin, M., et al., The quasi-biennial oscillation, *Rev. Geophys.*, *39*, 179–229, 2001.

Beres, J., M. Alexander, and J. Holton, Effects of tropospheric wind shear on the spectrum of convectively generated gravity waves, *J. Atmos. Sci.*, *59*, 1805–1824, 2002.

Bevington, P., and D. Robinson, *Data Reduction and Error Analysis for the Physical Sciences*, 2nd ed., McGraw Hill, New York, 1992.

Brewer, A., Evidence for a world circulation provided by the measurements of helium and water vapor distribution in the straosphere, *Q. J. R. Meteorol. Soc.*, *75*, 351–363, 1949.

Butchart, N., and J. Austin, Middle atmosphere climatologies from the troposphere-stratosphere configuration of the ukmo's unified model, *J. Atmos. Sci.*, *55*, 2782–2809, 1998.

Charron, M., E. Manzini, and C. Warner, Intercomparison of gravity wave parameterizations: Hines doppler-spread and warner and mcintyre ultra-simple schemes, *J. Meteorol. Soc. Jpn.*, *80*, 335–345, 2002.

Dewan, E., and R. Good, Saturation and the "universal" spectrum for vertical profiles of horizontal scalar winds in the atmosphere, *J. Geophys. Res.*, *91*, 2742–2748, 1986.

Dewan, E., R. Picard, R. O'Neil, H. Gardiner, J. Gibson, J. Mill, E. Richards, M. Kendra, and W. Gallery, Msx satellite observations of thunderstorm-generated gravity waves in mid-wave infrared images of the upper stratosphere, *Geophys. Res. Lett.*, *25*, 939–942, 1998.

Dunkerton, T., Theory of the mesopause semiannual oscillation, *J. Atmos. Sci.*, *39*, 2681–2690, 1982.

Dunkerton, T., The role of gravity waves in the quasi-biennial oscillation, *J. Geophys. Res.*, *102*, 26,053–26,076, 1997.

Eckermann, S., and P. Preusse, Global measurements of stratospheric mountain waves from space, *Science*, *286*, 1534–1537, 1999.

Fetzer, E. J., and J. C. Gille, Gravity wave variance in lims temperatures, i. Variability and comparison with background winds, *J. Atmos. Sci.*, *51*, 2461–2483, 1994.

Fritts, D. C., and W. Lu, Spectral estimates of gravity wave energy and momentum fluxes, ii: Parameterization of wave forcing and variability, *J. Atmos. Sci.*, *50*, 3695–3713, 1993.

Garcia, R., and B. A. Boville, "downward control" of the mean meridional circulation and temperature distribution of the polar winter stratosphere, *J. Atmos. Sci.*, *51*, 2238–2245, 1994.

Garcia, R., and F. Sassi, Modulation of the mesospheric semiannual oscillation by the quasibiennial oscillation, *Earth Planets Space*, *51*, 563–570, 1999.

Giorgetta, M., E. Manzini, and E. Roeckner, Forcing of the quasi-biennial oscillation from a broad spectrum of atmospheric waves, *Geophys. Res. Lett.*, *29*, 8-61–8-64, 2002.

Hamilton, K., Diagnostic study of the momentum balance in the Northern Hemisphere winter stratosphere, *Mon. Weather Rev.*, *111*, 1434–1441, 1983.

Hamilton, K., R. Wilson, and R. Hemler, Middle atmosphere simulated with high vertical and horizontal resolution versions of a gcm: Improvements in the cold pole bias and generation of a qbo-like oscillation in the tropics, *J. Atmos. Sci.*, *56*, 3829–3846, 1999.

Hartmann, D., The dynamical climatology of the stratosphere in the Southern Hemisphere during late winter 1973, *J. Atmos. Sci.*, *33*, 1789–1802, 1976.

Haynes, P. H., C. J. Marks, M. E. McIntyre, T. G. Shepherd, and K. P. Shine, On the "downward control" of extratropical diabatic circulations by eddy-induced mean zonal forces, *J. Atmos. Sci.*, *48*, 651–678, 1991.

Hertzog, A., F. Vial, A. Drnbrack, S. D. Eckermann, B. M. Knudsen, and J.-P. Pommereau, In situ observations of gravity waves and comparisons with numerical simulations during the SOLVE/THESEO 2000 campaign, *J. Geophys. Res.*, *107*(D20), 8292, doi:10.1029/2001JD001025, 2002.

Hines, C., Doppler-spread parameterization of gravity-wave momentum deposition in the middle atmosphere. 1. Basic formulation, *J. Atmos. Sol. Terr. Phys.*, *59*, 371–386, 1997.

Hitchman, M., and C. Leovy, Evolution of the zonal mean state in the equatorial middle atmosphere during october 1978–may 1979, *J. Atmos. Sci.*, *43*, 3159–3176, 1986.

Holton, J., M. Alexander, and M. Boehm, Evidence for short vertical wavelength kelvin waves in the doe-arm nauru99 radiosonde data, *J. Geophys. Res.*, *106*, 20,125–20,129, 2001.

Holton, J., J. Beres, and X. Zhou, On the vertical scale of gravity waves excited by localized thermal forcing, *J. Atmos. Sci.*, *59*, 2019–2023, 2002.

Jackson, D. R., and L. J. Gray, Simulation of the semi-annual oscillation of the equatorial middle atmosphere using the extended ugamp general circulation model, *Q. J. R. Meteorol. Soc.*, *120*, 1559–1588, 1994.

Larsen, M. F., W. E. Swartz, and R. Woodman, Gravity-wave generation by thunderstorms observed with a vertically-pointing 430 mhz radar, *Geophys. Res. Lett.*, *9*, 571–574, 1982.

Lighthill, J., *Waves in Fluids*, Cambridge Univ. Press, New York, 1978.

Lindzen, R., Wave-mean flow interactions in the upper atmosphere, *Boundary Layer Meteorol.*, *4*, 327–343, 1973.

Lindzen, R., Turbulence and stress owing to gravity wave and tidal breakdown, *J. Geophys. Res.*, *86*, 9707–9714, 1981.

Lindzen, R., and J. R. Holton, A theory of the quasi-biennial oscillation, *J. Atmos. Sci.*, *25*, 1095–1107, 1968.

McFarlane, N. A., The effect of orographically excited gravity wave drag on the general circulation of the lower stratosphere and troposphere, *J. Atmos. Sci.*, *44*, 1775–1800, 1987.

McLandress, C., On the importance of gravity waves in the middle atmosphere and their parameterization in general circulation models, *J. Atmos. Sol. Terr. Phys.*, *60*, 1357–1383, 1998.

McLandress, C., M. J. Alexander, and D. Wu, Microwave limb sounder observations of gravity waves in the stratosphere: A climatology and interpretation, *J. Geophys. Res.*, *105*, 11,947–11,967, 2000.

Medvedev, A., and G. Klaassen, Vertical evolution of gravity wave spectra and the parameterization of associated wave drag, *J. Geophys. Res.*, *100*, 25,841–25,853, 1995.

Mote, P., T. Dunkerton, M. McIntyre, E. Ray, P. Haynes, I. Russell, and J. M., Vertical velocity, vertical diffusion, and dilution by midlatitude air in the tropical lower stratosphere, *J. Geophys. Res.*, *103*, 8651–8666, 1998.

Murgatroyd, R., and F. Singleton, Possible meridional circulations in the stratosphere and mesosphere, *Q. J. R. Meteorol. Soc.*, *87*, 125–135, 1961.

Olaguer, E., H. Yang, and K. Tung, A reexamination of the radiative balance of the stratosphere, *J. Atmos. Sci.*, *49*, 1242–1263, 1992.

Palmer, T. N., G. J. Shutts, and R. Swinbank, Alleviation of a systematic westerly bias in general circulation and numerical weather prediction models through an orographic gravity wave drag parameterization, *Q. J. R. Meteorol. Soc.*, *112*, 1001–1039, 1986.

Pawson, S. E. A., The gcm-reality intercomparison project for sparc (grips): Scientific issues and initial results, *Bull. Am. Meteorol. Soc.*, *81*, 781–796, 2000.

Pfister, L., K. R. Chan, T. P. Bui, S. Bowen, M. Legg, B. Gary, K. Kelly, M. Proffitt, and W. Starr, Gravity waves generated by a tropical cyclone during the step tropical feild program: A case study, *J. Geophys. Res.*, *98*, 8611–8638, 1993.

Preusse, P., B. Schaeler, J. Bacmeister, and D. Offermann, Evidence for gravity waves in crista temperatures, *Adv. Space Res.*, *24*, 1601–1604, 1999.

Preusse, P., S. Eckermann, and D. Offermann, Comparison of global distributions of zonal-mean gravity wave variance inferred from different satellite instruments, *Geophys. Res. Lett.*, *27*, 3877–3880, 2000.

Ray, E., M. Alexander, and J. Holton, An analysis of the structure and forcing of the equatorial semiannual oscillation in zonal wind, *J. Geophys. Res.*, *103*, 1759–1774, 1998.

Rosenlof, K., Seasonal cycle of the residual mean meridional circulation in the stratosphere, *J. Geophys. Res.*, *100*, 5173–5191, 1995.

Rosenlof, K., Summer hemisphere differences in temperature and transport in the lower stratosphere, *J. Geophys. Res.*, *101*, 19,129–19,136, 1996.

Rosenlof, K. H., and J. R. Holton, Estimates of the stratospheric residual circulation using the downward control principle, *J. Geophys. Res.*, *98*, 10,465–10,479, 1993.

Sassi, F., and R. Garcia, The role of equatorial waves forced by convection in the tropical semiannual oscillation, *J. Atmos. Sci.*, *54*, 1925–1942, 1997.

Sato, K., Vertical wind disturbances in the afternoon of mid-summer revealed by the mu radar, *Geophys. Res. Lett.*, *19*, 1943–1946, 1992.

Sato, K., A statistical study of the structure, saturation and sources of inertio-gravity waves in the lower stratosphere observed with the mu radar, *J. Atmos. Terr. Phys.*, *56*, 755–774, 1994.

Sato, K., and T. Dunkerton, Estimates of momentum flux associated with equatorial kelvin and gravity waves, *J. Geophys. Res.*, *102*, 26,247–26,261, 1997.

Sato, K., H. Hashiguchi, and S. Fukao, Gravity waves and turbulence associated with cumulus convection observed with the uhf/vhf clear-air doppler radars, *J. Geophys. Res.*, *100*, 7111–7120, 1995.

Scaife, A., N. Butchart, C. Warner, D. Stainforth, and W. Norton, Realistic quasi-biennial osciallations in a simulation of the global climate, *Geophys. Res. Lett.*, *27*, 3481–3484, 2000.

Scaife, A., N. Butchart, C. Warner, and R. Swinbank, Impact of a spectral gravity wave parameerization on the stratosphere in the met office unified model, *J. Atmos. Sci.*, *59*, 1473–1489, 2002.

Smith, A., and L. Lyjak, An observational estimate of gravity wave drag from the momentum balance in the middle atmosphere, *J. Geophys. Res.*, *90*, 2233–2241, 1985.

Swinbank, R., and A. O'Neill, A stratosphere-troposphere data assimilation system, *Mon. Weather Rev.*, *122*, 686–702, 1994a.

Swinbank, R., and A. O'Neill, Quasi-biennial and semi-annual oscillations in equatorial wind fields constructed by data assimilation, *Geophys. Res. Lett.*, *21*, 2099–2102, 1994b.

Takahashi, M., and B. A. Boville, A three-dimensional simulation of the equatorial quasi-biennial oscillation, *J. Atmos. Sci.*, *49*, 1020–1035, 1992.

Tsuda, T., M. Nishida, C. Rocken, and R. Ware, A global morphology of gravity wave activity in the stratosphere revealed by the gps occultation data (gps/met), *J. Geophys. Res.*, *105*, 7257–7274, 2000.

Vial, F., A. Hertzog, C. Mechoso, C. Basdevant, P. Cocquerez, V. Dubourg, and F. Nouel, A study of the dynamics of the equatorial lower stratosphere by use of ultra long duration balloons: 1. Planetary scales, *J. Geophys. Res.*, *106*, 22,725–22,744, 2001.

Vincent, R., and M. Alexander, Gravity waves in the tropical lower stratosphere: An observational study of seasonal and interannual variability, *J. Geophys. Res.*, *105*, 17,971–17,982, 2000.

Wada, K., T. Nitta, and K. Sato, Equatorial inertia-gravity waves in the lower stratosphere revealed by toga-coare iop data, *J. Meteorol. Soc. Jpn.*, *77*, 721–736, 1999.

Warner, C., and M. McIntyre, An ultra-simple spectral parameterization for non-orographic gravity waves, *J. Atmos. Sci.*, *58*, 1837–1857, 2001.

Whiteway, J., T. Duck, D. Donovan, J. Bird, S. Pal, and A. Carswell, Measurements of gravity wave activity within and around the arctic stratospheric vortex, *Geophys. Res. Lett.*, *24*, 1387–1390, 1997.

Worthington, R., Alignment of mountain wave patterns above wales: A vhf radar study during 1990–1998, *J. Geophys. Res.*, *104*, 9199–9212, 1999.

Wu, D., and J. Waters, Gravity-wave-scale temperature fluctuations seen by the uars mls, *Geophys. Res. Lett.*, *23*, 3289–3292, 1996a.

Wu, D., and J. Waters, Satellite observations of atmospheric variances: A possible indication of gravity waves, *Geophys. Res. Lett.*, *23*, 3631–3634, 1996b.

Yulaeva, E., J. R. Holton, and J. M. Wallace, On the cause of the annual cycle in the tropical lower stratospheric temperature, *J. Atmos. Sci.*, *51*, 169–174, 1994.

M. J. Alexander, Colorado Research Associates, Division of Northwest Research Associates, 3380 Mitchell Lane, Boulder, CO 80301, USA. (alexand@colorado-research.com)

K. H. Rosenlof, NOAA Aeronomy Laboratory, Boulder, CO 80303, USA. (krosenlof@al.noaa.gov)